PHYSICAL REVIEW D **95,** 043009 (2017)

Polytropic spheres containing regions of trapped null geodesics

Jan Novotný,[*] Jan Hladík,[†] and Zdeněk Stuchlík[‡]

Institute of Physics and Research Centre of Theoretical Physics and Astrophysics, Faculty of Philosophy and Science, Silesian University in Opava, Bezručovo náměstí 13, CZ-746 01 Opava, Czech Republic

(Received 22 December 2016; published 28 February 2017)

We demonstrate that in the framework of standard general relativity, polytropic spheres with properly fixed polytropic index n and relativistic parameter σ, giving a ratio of the central pressure p_c to the central energy density ρ_c, can contain a region of trapped null geodesics. Such trapping polytropes can exist for $n > 2.138$, and they are generally much more extended and massive than the observed neutron stars. We show that in the n–σ parameter space, the region of allowed trapping increases with the polytropic index for intervals of physical interest, $2.138 < n < 4$. Space extension of the region of trapped null geodesics increases with both increasing n and $\sigma > 0.677$ from the allowed region. In order to relate the trapping phenomenon to astrophysically relevant situations, we restrict the validity of the polytropic configurations to their extension $r_{\rm extr}$ corresponding to the gravitational mass $M \sim 2M_\odot$ of the most massive observed neutron stars. Then, for the central density $\rho_c \sim 10^{15}$ g cm^{-3}, the trapped regions are outside $r_{\rm extr}$ for all values of $2.138 < n < 4$; for the central density $\rho_c \sim 5 \times 10^{15}$ g cm^{-3}, the whole trapped regions are located inside $r_{\rm extr}$ for $2.138 < n < 3.1$; while for $\rho_c \sim 10^{16}$ g cm^{-3}, the whole trapped regions are inside $r_{\rm extr}$ for all values of $2.138 < n < 4$, guaranteeing astrophysically plausible trapping for all considered polytropes. The region of trapped null geodesics is located close to the polytrope center and could have a relevant influence on the cooling of such polytropes or binding of gravitational waves in their interior.

DOI: 10.1103/PhysRevD.95.043009

I. INTRODUCTION

Extremely compact objects having surface R located under the radius $r_{\rm ph}$ of photon circular geodesics of the external Schwarzschild (or some generalized spherically symmetric vacuum) spacetime are important because they have to contain a region of trapped null geodesics that could be relevant for trapping of gravitational waves [1], or radiated neutrinos [2]. The existence of extremely compact objects has been demonstrated in the physically implausible, but principally very interesting case of spheres with uniform distribution of energy density (but radii-dependent distribution of pressure) [3–6]. However, the models of neutron or quark stars based on the known realistic equations of state do not allow for the existence of extremely compact objects defined in this way, as in the most extreme cases, $R \geq 3.5M > r_{\rm ph} = 3M$, where M denotes the mass of the compact star [7].

Surprisingly, a recent study related to the general relativistic polytropic spheres in spacetimes with a repulsive cosmological constant demonstrates the possibility to obtain relativistic polytropic spheres containing, near their center, a region with trapped null geodesics [8]. This is an important result, as the surfaces of such polytropes can be located above $r_{\rm ph} = 3M$ so we could reconsider the definition of the extremely compact objects, restricting our attention solely to the existence of a trapped null geodesics region. Although the polytropic spheres represent some physical idealization, it is well known that they represent nonrelativistic ($n = 1.5$) and ultrarelativistic ($n = 3$) degenerated Fermi gas that can be taken quite seriously, as it is physically interesting, especially for the ultrarelativistic Fermi gas [9].

For this reason, we study in detail the existence of general relativistic polytropes containing a region of trapped null geodesics. The role of the cosmological constant is relevant only for very extended objects with radii close to the static radius of the external spacetime [10–12] and low central density [8]. Thus, it is clear that it will be irrelevant for our study, and we can abandon the influence of the cosmological constant. In order to find the regions of trapped null geodesics, we use, following Ref. [8], the construction of the so-called optical geometry, related to the polytrope internal spacetime, and its embedding diagrams. This is a quite efficient method, as in the spherically symmetric spacetimes, the turning points of the optical geometry embedding diagrams correspond to the stable and unstable photon circular geodesics, implying the existence of a region of trapped null geodesics [13]. We relate the general discussion of the trapping polytropes to situations of direct astrophysical relevance, demonstrating their strong dependence on the central energy density and restricting the validity of the polytropic state equations to regions giving masses smaller than the observational limit

[*]jan.novotny@fpf.slu.cz
[†]jan.hladik@fpf.slu.cz
[‡]zdenek.stuchlik@fpf.slu.cz

of the neutron star mass ($M \sim 2M_\odot$). We present a detailed discussion for the case of the ultrarelativistic Fermi gas with polytropic index $n = 3$.

II. POLYTROPE STRUCTURE EQUATIONS

For a spherically symmetric, static spacetime, expressed in terms of the standard Schwarzschild coordinates, the line element takes the form

$$ds^2 = -e^{2\Phi}c^2dt^2 + e^{2\Psi}dr^2 + r^2(d\theta^2 + \sin^2\theta d\phi^2). \quad (1)$$

The metric has two unknown functions of the radial coordinate, $\Phi(r)$ and $\Psi(r)$. The static configuration is assumed to be a perfect fluid having the stress-energy tensor

$$T^\mu{}_\nu = (p + \rho c^2)U^\mu U_\nu + p\delta^\mu_\nu, \quad (2)$$

where U^μ denotes the 4-velocity of the fluid. In the fluid rest frame, $\rho = \rho(r)$ represents the mass-energy density and $p = p(r)$ represents the isotropic pressure.

We assume the mass-energy density and pressure related by the polytropic equation of state

$$p = K\rho^{1+1/n}, \quad (3)$$

where the constant n denotes the polytropic index. K denotes a constant governed by the thermal characteristics of a given polytropic configuration by specifying the density ρ_c and pressure p_c at its center—it is determined by the total mass and radius of the configuration, and the relativistic parameter [14]

$$\sigma \equiv \frac{p_c}{\rho_c c^2} = \frac{K}{c^2}\rho_c^{1/n}. \quad (4)$$

For a given pressure, the density is a function of temperature. Therefore, the constant K contains the temperature implicitly. The polytropic equation is a limiting form of the parametric equations of state for the completely degenerate gas at zero temperature that can be relevant, e.g., for neutron stars. In such a situation, both n and K are universal physical constants [14]. The polytropic law assumption enables one to describe the basic properties of the fluid configurations governed by the relativistic laws. The equation of state of the ultrarelativistic degenerate Fermi gas is determined by the polytropic equation, with the adiabatic index $\Gamma = 4/3$ corresponding to the polytropic index $n = 3$, while the nonrelativistic degenerate Fermi gas is determined by the polytropic equation of state with $\Gamma = 5/3$ and $n = 3/2$ [9].

The structure equations of the general relativistic polytropic spheres are determined by the Einstein field equations

$$R_{\mu\nu} - \frac{1}{2}Rg_{\mu\nu} = \frac{8\pi G}{c^4}T_{\mu\nu}, \quad (5)$$

and by the local energy-momentum conservation law

$$T^{\mu\nu}{}_{;\nu} = 0. \quad (6)$$

The structure of the polytropic spheres is governed by the two structure functions. The first one, $\theta(r)$, is related to the mass-energy density radial profile $\rho(r)$ and the central density ρ_c [14],

$$\rho = \rho_c\theta^n, \quad (7)$$

with the boundary condition $\theta(r = 0) = 1$. The second one is the mass function given by the relation

$$m(r) = \int_0^r 4\pi r^2\rho dr, \quad (8)$$

with the integration constant chosen to be $m(0) = 0$, to guarantee the smooth spacetime geometry at the origin [15]. At the surface of the configuration at $r = R$, we get $\rho(R) = p(R) = 0$, the total mass of the polytropic configuration $M = m(R)$. Outside the polytropic configuration, the spacetime is described by the vacuum Schwarzschild metric.

The structure equations of the polytropic spheres related to the two structure functions $\theta(r)$ and $m(r)$ and the parameters n, σ can be put into the form [8,14]

$$\frac{\sigma(n+1)}{1+\sigma\theta}r\frac{d\theta}{dr}\left(1 - \frac{2Gm(r)}{c^2 r}\right) + \frac{Gm(r)}{c^2 r} = -\frac{G}{c^2}\sigma\theta\frac{dm}{dr}, \quad (9)$$

$$\frac{dm}{dr} = 4\pi r^2\rho_c\theta^n. \quad (10)$$

Introducing the characteristic length scale $\mathcal{L}$ of the polytropic sphere [14],

$$\mathcal{L} = \left[\frac{(n+1)K\rho_c^{1/n}}{4\pi G\rho_c}\right]^{1/2} = \left[\frac{\sigma(n+1)c^2}{4\pi G\rho_c}\right]^{1/2}, \quad (11)$$

and the characteristic mass scale $\mathcal{M}$ of the polytropic sphere,

$$\mathcal{M} = 4\pi\mathcal{L}^3\rho_c = \frac{c^2}{G}\sigma(n+1)\mathcal{L}, \quad (12)$$

the structure equations, Eqs. (9) and (10), can be transformed into a dimensionless form by introducing a dimensionless radial coordinate

$$\xi = \frac{r}{\mathcal{L}}, \quad (13)$$

and a dimensionless gravitational mass function

$$v(\xi) = \frac{m(r)}{4\pi\mathcal{L}^3\rho_c}. \tag{14}$$

The dimensionless structure equations then take the form (for details, see Refs. [8,14])

$$\xi^2 \frac{d\theta}{d\xi} \frac{1 - 2\sigma(n+1)(v/\xi)}{1+\sigma\theta} + v(\xi) = -\sigma\xi\theta\frac{dv}{d\xi}, \tag{15}$$

$$\frac{dv}{d\xi} = \xi^2\theta^n. \tag{16}$$

For fixed parameters n, σ, the structure equations (15) and (16) have to be simultaneously solved under the boundary conditions

$$\theta(0) = 1, \qquad v(0) = 0. \tag{17}$$

From Eqs. (16) and (17), it follows that $v(\xi) \sim \xi^3$ for $\xi \to 0$ and, according to Eq. (15), we obtain

$$\lim_{\xi\to 0_+} \frac{d\theta}{d\xi} = 0. \tag{18}$$

The surface of the polytropic sphere, $r = R$, is represented by the first zero point of $\theta(\xi)$, denoted as ξ_1:

$$\theta(\xi_1) = 0. \tag{19}$$

Therefore, the solution ξ_1 determines the surface radius of the polytropic sphere, and the solution $v(\xi_1)$ determines its gravitational mass.

The solutions of the polytropic structure equations can be obtained by numerical methods only [14], with the exception of the $n = 0$ polytropes governing the spheres with a uniform distribution of the energy density when the solution can be given in terms of the elementary functions [3,8].

III. CHARACTERISTICS OF THE POLYTROPIC SPHERES

A polytropic sphere constructed for given parameters n, σ and ρ_c is characterized by two solutions of the structure equations ξ_1 and $v(\xi_1)$ and by the scale factors $\mathcal{L}$ and $\mathcal{M}$. Then, the radius of the polytropic sphere reads

$$R = \mathcal{L}\xi_1, \tag{20}$$

while the gravitational mass of the sphere is given by

$$M = \mathcal{M}v(\xi_1) = \frac{c^2}{G}\mathcal{L}\sigma(n+1)v(\xi_1). \tag{21}$$

The radial profiles of the energy density, pressure, and mass distribution are given by the relations

$$\rho(\xi) = \rho_c\theta^n(\xi), \tag{22}$$

$$p(\xi) = \sigma\rho_c\theta^{n+1}(\xi), \tag{23}$$

$$M(\xi) = M\frac{v(\xi)}{v(\xi_1)}. \tag{24}$$

The temporal metric coefficient takes the form

$$e^{2\Phi_{int}} = (1+\sigma\theta)^{-2(n+1)}\left\{1 - 2\sigma(n+1)\frac{v(\xi_1)}{\xi_1}\right\}, \tag{25}$$

and the radial metric coefficient takes the form

$$e^{-2\Psi_{int}} = 1 - 2\sigma(n+1)\frac{v(\xi)}{\xi}. \tag{26}$$

Detailed discussion of the polytropic spheres, including their gravitational binding energy and the internal energy, can be found in Refs. [8,14].

The compactness parameter governing the effectiveness of the gravitational binding of the polytropic spheres is given by the relation

$$\mathcal{C} \equiv \frac{GM}{c^2R} = \frac{1}{2}\frac{r_g}{R} = \frac{\sigma(n+1)v(\xi_1)}{\xi_1}, \tag{27}$$

where we have introduced the standard gravitational radius of the polytropic sphere that reflects its gravitational mass in length units,

$$r_g = \frac{2GM}{c^2}. \tag{28}$$

The compactness $\mathcal{C}$ of the polytropic sphere can be represented by the gravitational redshift of radiation emitted from the surface of the polytropic sphere [6].

All the characteristic functions introduced above can only be determined by numerical procedures for the polytropic equations of state with $n > 0$. The special case of polytropes with $n = 0$ corresponds to the physically unrealistic polytropic configurations with a uniform distribution of energy density; their characteristic functions can be given in terms of elementary functions, and they could serve as a test bed for more complex general polytropes [3,8].

The external vacuum of the polytropic sphere is represented by the Schwarzschild spacetime with the same gravitational mass parameter M as those characterizing the internal spacetime of the polytropic sphere, and it is given by the metric coefficients

$$e^{2\Phi_{ext}} = e^{-2\Psi_{ext}} = 1 - \frac{2GM}{c^2r}. \tag{29}$$

The photon sphere of the Schwarzschild spacetime, given by the photon circular geodesics, is located at the radius [15]

$$r_{\rm ph} = \frac{3GM}{c^2} = \frac{3}{2} r_{\rm g}. \tag{30}$$

In the following, we compare the radius of the obtained polytropic spheres containing a region of trapped null geodesics to this radius of the photon sphere in order to test if the original definition of the extremely compact objects ($R < r_{\rm ph}$) is satisfied. The relevant condition then reads $C > 1/3$.

In order to have a deeper insight into the character of polytropes containing a region of trapped null geodesics, we also consider the locally defined compactness of the polytrope, related to a given radius $r = \mathcal{L}\xi$ and given by the relation

$$\mathcal{C}(\xi) \equiv \frac{\sigma(n+1)v(\xi)}{\xi}. \tag{31}$$

We can then test if the condition $C(\xi) > 1/3$ is satisfied inside the trapping polytropes.

IV. EMBEDDINGS OF THE OPTICAL GEOMETRY RELATED TO POLYTROPIC SPHERES

We concentrate our attention on the visualization of the structure of the internal spacetime of the general relativistic polytropes, considering the optical geometry of the spacetime. Such a visualization enables us to easily find the polytropic structures containing a region of trapped null geodesics.

A. Embedding diagrams

The curvature of the internal spacetime of the polytropes can conveniently be represented by the standard embedding of 2D, appropriately chosen, spacelike surfaces of the ordinary 3-space of the geometry (here, these are $t = \text{const}$ sections of the central planes) into 3D Euclidean space [15].

The 3D optical reference geometry [16] related to the spacetime under consideration enables us to introduce a natural "Newtonian" concept of gravitational and inertial forces, reflecting some hidden properties of the test particle motion [13,17–19]. For an alternative approach to the concept of inertial forces, see, e.g., the "special relativistic" one [20]. Properties of the inertial forces are reflected by the embedding diagrams of appropriate 2D sections of the optical geometry. The embedding diagrams of the $n = 0$ polytropes were presented in Ref. [4]; here, they are applied for relativistic polytropes with $n > 0$. Note that using the optical reference geometry, it can be shown that extremely compact configurations allowing the existence of bound null geodesics exist [4,21]. For the extremely compact relativistic polytropes with trapped null geodesics, a turning point of the embedding diagram of the optical geometry occurs [13].

We embed the equatorial plane of the optical reference geometry into the 3D Euclidean space with the line element

$$\mathrm{d}\tilde{\sigma}^2 = \mathrm{d}\rho^2 + \rho^2 \mathrm{d}\alpha^2 + \mathrm{d}z^2. \tag{32}$$

The embedding is represented by a rotationally symmetric surface $z = z(\rho)$ with the 2D line element

$$\mathrm{d}\ell^2_{\rm (E)} = \left[1 + \left(\frac{\mathrm{d}z}{\mathrm{d}\rho}\right)^2\right]\mathrm{d}\rho^2 + \rho^2 \mathrm{d}\alpha^2. \tag{33}$$

B. Optical reference geometry

In the static spacetimes, the metric coefficients of the optical 3D space are determined by [16]

$$h_{ik} = \frac{g_{ik}}{-g_{tt}}. \tag{34}$$

In the equatorial plane, the line element has the form

$$\mathrm{d}\ell^2_{\rm (opt)} = h_{rr}\mathrm{d}r^2 + h_{\phi\phi}\mathrm{d}\phi^2 \tag{35}$$

which has to be identified with $\mathrm{d}\ell^2_{\rm (E)}$. The azimuthal coordinates of the optical space and the Euclidean space can be identified ($\alpha \equiv \phi$), but the radial coordinates are related by

$$\rho^2 = h_{\phi\phi}. \tag{36}$$

Then, the embedding formula is determined by

$$\left(\frac{\mathrm{d}z}{\mathrm{d}\rho}\right)^2 = h_{rr}\left(\frac{\mathrm{d}r}{\mathrm{d}\rho}\right)^2 - 1. \tag{37}$$

We transform the embedding formula into a parametric form $z(\rho) = z(r(\rho))$, implying

$$\frac{\mathrm{d}z}{\mathrm{d}r} = \sqrt{h_{rr} - \left(\frac{\mathrm{d}\rho}{\mathrm{d}r}\right)^2}. \tag{38}$$

The turning points of the embedding diagrams are given by the condition [13]

$$\frac{\mathrm{d}\rho}{\mathrm{d}r} = 0. \tag{39}$$

We also have to take into consideration the so-called reality condition determining the limits of embeddability,

$$h_{rr} - \left(\frac{\mathrm{d}\rho}{\mathrm{d}r}\right)^2 \geq 0. \tag{40}$$

C. Embeddings of the polytrope optical geometry

For the general relativistic polytropes, the metric coefficients of the optical geometry take the form

$$h_{rr} = \frac{e^{2\Psi}}{e^{2\Phi}} = \frac{[1+\sigma\theta(\xi)]^{2(n+1)}}{1-2\sigma(n+1)v(\xi_1)/\xi_1} \times \left\{1-2\sigma(n+1)\frac{v(\xi)}{\xi}\right\}^{-1}, \quad (41)$$

$$h_{\phi\phi} = \frac{r^2}{e^{2\Phi}} = \frac{r^2[1+\sigma\theta(\xi)]^{2(n+1)}}{1-2\sigma(n+1)v(\xi_1)/\xi_1}. \quad (42)$$

It is convenient to introduce new dimensionless coordinates η and $\tilde{z}$ by

$$\eta = \frac{\rho}{\mathcal{L}}, \qquad \tilde{z} = \frac{z}{\mathcal{L}}. \quad (43)$$

Then, we can write

$$\eta = \frac{\xi[1+\sigma\theta(\xi)]^{n+1}}{\left[1-2\sigma(n+1)\frac{v(\xi_1)}{\xi_1}\right]^{1/2}} \quad (44)$$

and

$$\frac{d\eta}{d\xi} = \frac{\left[1+\sigma\theta(\xi)\right]^n\left\{1+\sigma[\theta(\xi)+(n+1)\xi\frac{d\theta}{d\xi}\right\}}{\left[1-2\sigma(n+1)\frac{v(\xi_1)}{\xi_1}\right]^{1/2}}. \quad (45)$$

The condition governing the turning points of the embedding diagrams reads

$$\sigma\left[\theta(\xi)+(n+1)\xi\frac{d\theta}{d\xi}\right] = -1. \quad (46)$$

The embedding formula takes the form

$$\left(\frac{d\tilde{z}}{d\xi}\right)^2 = \left\{1-2\sigma(n+1)\frac{v(\xi_1)}{\xi_1}\right\}^{-1}\left\{1-2\sigma(n+1)\frac{v(\xi)}{\xi}\right\}^{-1} 2\sigma(n+1)[1+\sigma\theta(\xi)]^{2n} \times\left\{\left\{1+\sigma\left[\theta(\xi)+(n+1)\xi\frac{d\theta}{d\xi}\right]\right\}^2\frac{v(\xi)}{\xi}-\xi\frac{d\theta}{d\xi}\left[1+\sigma\theta(\xi)+\frac{\sigma}{2}(n+1)\xi\frac{d\theta}{d\xi}\right]\right\}. \quad (47)$$

The condition of embeddability giving the limits of applicability of the embedding procedure takes the form

$$\left\{1+\sigma\left[\theta(\xi)+(n+1)\xi\frac{d\theta}{d\xi}\right]\right\}^2\frac{v(\xi)}{\xi} - \xi\frac{d\theta}{d\xi}\left[1+\sigma\theta(\xi)+\frac{\sigma}{2}(n+1)\xi\frac{d\theta}{d\xi}\right] \geq 0. \quad (48)$$

Notice that the embedding diagrams are purely related to the solutions of the dimensionless structure equations of the general relativistic polytropes, which are independent of the length scale factor $\mathcal{L}$ governing the physical extension and gravitational mass of the polytropes. For this reason, the existence of the zones of null geodesics trapping will also be independent of the length scale factor $\mathcal{L}$. The trapping phenomenon is thus fully governed by the polytrope parameters n and σ—it is formally independent of the central density ρ_c that enters the definition of the relativistic parameter σ.

Using numerically obtained solutions of the polytrope structure equations, we give examples of the embedding diagrams. In Fig. 1, the embedding diagram of the optical geometry of the internal $n = 3$ polytrope spacetime is given for the extremal value of the relativistic parameter $\sigma = 3/4$ allowed by the causality limit [14]. As demonstrated in Ref. [13], the turning points of the diagram correspond to the (inner) stable null circular geodesics at radius $r_{ph(s)} = r_c$ and to the (outer) unstable null circular geodesic at radius $r_{ph(u)} = r_b$. The radius r_c corresponds to the center of the trapping region, while the radius r_b corresponds to its outer boundary. In Fig. 2, we demonstrate how the optical geometry embeddings depend on the polytrope index n and on the relativistic parameter σ for fixed n. In the next section, we use the embeddings for a detailed study of the existence of the trapping zones for null geodesics polytropic parameters n and σ.

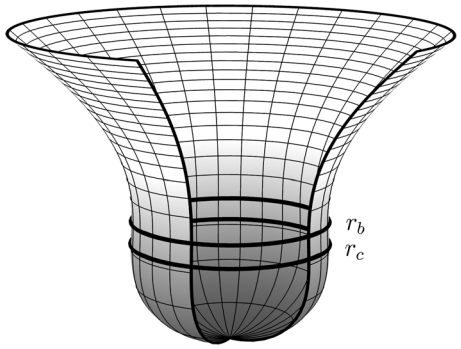

FIG. 1. Optical geometry of the polytropic sphere having $n = 3$ and $\sigma = 3/4$. The turning points corresponding to the stable and unstable null circular geodesics are depicted as circles r_c and r_b.

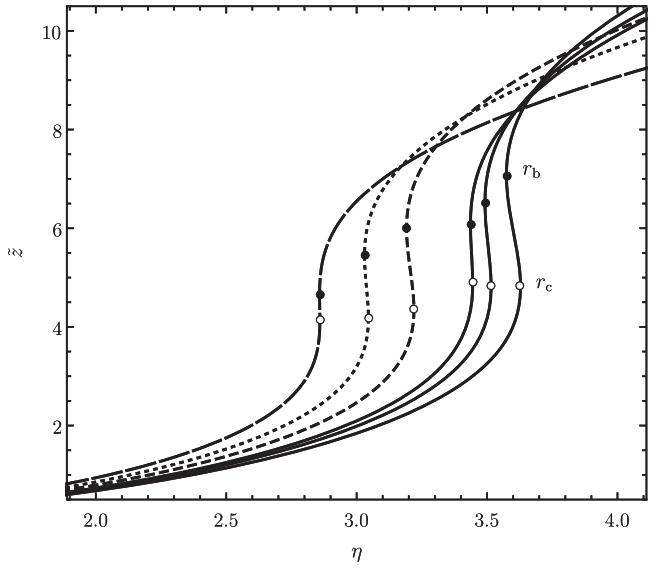

FIG. 2. Embedding diagram constructed for several polytropic spheres having the polytropic and relativistic parameters $\{n, \sigma\}$ valued gradually as $\{2.2, 11/16\}$, $\{2.5, 5/7\}$, $\{2.7, 27/37\}$, $\{3, 7/10\}$, $\{3, 18/25\}$, $\{3, 3/4\}$ (curves in the same order as the growing η coordinate of the turning points r_c and r_b corresponding to null circular geodesics).

V. GENERAL RELATIVISTIC POLYTROPES CONTAINING A REGION OF TRAPPED NULL GEODESICS

Numerical solutions of the structure equations of the polytrope spheres yield the dimensionless radial profiles of energy density, mass and metric coefficients, and the dimensionless extension and mass parameters ξ_1 and $v_1 = v_{\xi_1}$. These solutions are governed by the parameters n and σ, since they are independent of the third parameter governing the polytrope spheres, ρ_c, that governs the length and mass scales of the polytropes. We restrict our attention to the polytropic spheres with the standard choice of the polytropic index, $0 \leq n \leq 4$.

A. Demarcation of trapping region in n–σ parameter space

As demonstrated in the previous section, a region with trapped null geodesics can exist in the interior of the polytropic spheres, if the parameters n and σ are conveniently chosen. Thus, we first give the region of the n–σ parameter space, determining the polytropic spheres demonstrating the trapping phenomenon.

First, we have to put the upper causal limit on the relativistic parameter. To avoid a superluminal speed of sound in the gas, a maximal value of the relativistic parameter σ for fixed polytropic index n is limited. For adiabatic processes in the polytropic spheres, the phase velocity of the sound is given by

$$v_s^2 = \left(\frac{dp}{dQ}\right)_{\text{adiabatic}}. \tag{49}$$

Because the radial profile of the pressure in any polytropic fluid sphere is a monotonically decreasing function, the limit on the maximum value of σ results from the restriction on the speed of sound in the center, thus giving the relation

$$v_{sc} \equiv c\left(\frac{n+1}{n}\sigma\right)^{1/2} < c. \tag{50}$$

Hence, for a given polytropic index n, one gets the upper limit restriction

$$\sigma \leq \frac{n}{n+1} \equiv \sigma_{\max}. \tag{51}$$

Using the behavior on the left-hand side of Eq. (46), denoted as the turning function $\sigma[\theta(\xi) + (n+1)\xi\frac{d\theta}{d\xi}] \equiv T(\xi; \sigma, n)$, we can numerically search for the existence of polytropic spheres demonstrating the trapping effect by solving the equation $T(\xi; \sigma, n) = -1$, as graphically depicted in Fig. 3 in the special case of $n = 3$ polytropes. If there are, for a fixed n, some values of σ implying two different solutions ξ_c and ξ_b of this equation, the trapping region exists, and the solutions give radii of the stable and unstable circular geodesics. We confirm this conclusion in the following by a direct study of the effective potential of the null geodesics of the internal spacetime of such polytropic configurations. If, for the fixed n, there is only one solution, where $\xi_c = \xi_b$, the minimal value of the relativistic parameter $\sigma_{\min}$ allowing for trapping is found. The numerical analysis demonstrates that the trapping region starts to exist for a properly selected relativistic

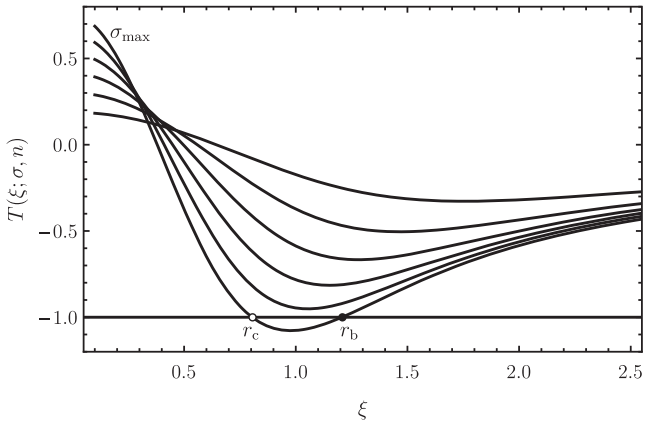

FIG. 3. Search of the critical relativistic parameter $\sigma_{\min}(n)$ and the turning points of the "turning" optical geometry embedding diagrams. If the turning function $T(\xi; \sigma, n) = -1$ for two different values of the coordinate ξ, the trapping effect exists for a given pair $\{n, \sigma\}$. Curves are depicted for $n = 3$. The parameter σ is gradually increased from the given nonzero value up to $\sigma_{\max}$. A similar behavior of plotted turning functions can also be seen for other values of the polytropic index $n > 2.138$.

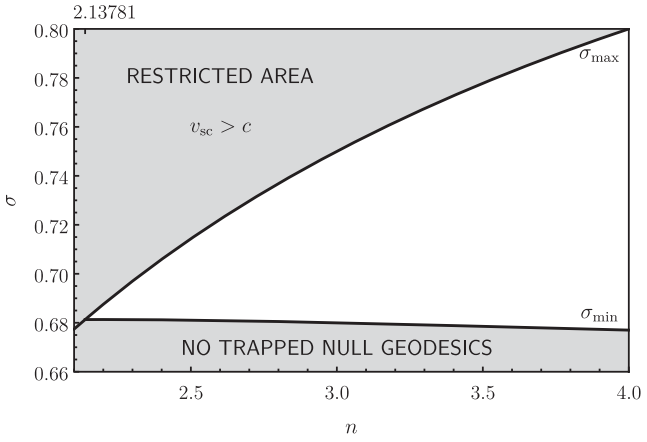

FIG. 4. Trapping polytropes in parameter n-σ space. We show the span of the possible parameter σ for a given polytropic index in the interval $2.138 < n < 4$ for which the trapping effect exists.

parameter σ, if the polytropic index overcomes the critical minimal value of $n_{\min} \doteq 2.1378$. The limiting maximal (and simultaneously minimal) allowed value of the relativistic parameter reads $\sigma_{\max}(n = 2.1378) = 0.681$.

Based on the above given procedure, the turning point limit $\sigma_{\min}(n)$ presented in Fig. 4 has been obtained. Together with the causal limit of $\sigma_{\max}(n)$, the turning point limit provides, in the parameter n–σ plane, a restriction on the existence of polytrophic spheres containing trapped null geodesics.

B. Physically relevant polytropic spheres

Now we can provide more detailed information on the physical properties of the polytropic spherical configurations containing regions of trapped null geodesics. For selected values of the polytropic index n and related maximal allowed values of the relativistic parameter $\sigma_{\max}(n)$, properties of such configurations—like the total gravitational mass, the surface radius, and the radii r_c and r_b governing the trapping zone of the polytrope—are summarized in Table I for the special selection of the central energy density of the polytropic sphere $\rho_c = 5 \times 10^{15}$ g cm^{-3}. We also give the ratio $\rho(r)/\rho_c$ at the radii $r = r_c$, $r = r_b$. Compactness of these polytropes will be studied separately.

Second, we put our results into an astrophysical context, related to the observational restrictions of the neutron stars, by considering the dependence of our general dimensionless results on the central energy density parameter ρ_c governing the extension and mass of the polytrope configuration. Note that all the characteristic radii and masses of the polytropic spheres depend significantly on the central energy density—when increasing the central density, the radii and masses decrease as $1/\sqrt{\rho_c}$.

Because of the observationally given limit on the mass of the neutron stars $M_{\max(o)} \sim 2M_\odot$ [7,22], we assume that the physical relevance of the polytropic equation of state is limited by the radius r_{extr} where the polytrope sphere reaches the mass $m(r_{\text{extr}}) = 2M_\odot$; above this radius, the sphere should be described by different equations of state, as is well known from the theory of neutron stars [9]. The maximum mass of neutron stars allowed theoretically by realistic equations of state is $M_{\max(t)} \sim 2.8M_\odot$ [23], while the minimal surface radius is $R_{\min} \sim 10$ km [24]. Moreover, we assume that the central energy density is supernuclear, i.e., $\rho_c > 10^{15}$ g cm^{-3}.

TABLE I. List of parameters describing a polytropic fluid sphere of given n having $\sigma = \sigma_{\max}$. For the calculation of the scale parameter $\mathcal{L}$, the value 5×10^{15} g cm^{-3} was used as ϱ_c.

n	$\sigma_{\max}$	R [km]	$M/M_\odot$	r_c [km]	$\varrho(r_c)/\varrho_c$	r_b [km]	$\varrho(r_b)/\varrho_c$	r_{extr} [km]	$\varrho(r_{\text{extr}})/\varrho_c$
4.0	0.80000	1.87×10^8	1251.82	6.2323	0.23344	11.0981	0.04914	9.9120	0.06835
3.9	0.79592	3.99×10^7	1102.78	6.2476	0.23275	10.9720	0.05055	9.8988	0.06840
3.8	0.79167	9.27×10^7	1602.90	6.2639	0.23200	10.8431	0.05205	9.8854	0.06843
3.7	0.78723	64276.3	54.1217	6.2813	0.23115	10.7111	0.05367	9.8719	0.06845
3.6	0.78261	21288.2	42.8887	6.3001	0.23021	10.5758	0.05541	9.8584	0.06843
3.5	0.77778	11280.6	34.6763	6.3203	0.22916	10.4370	0.05730	9.8448	0.06839
3.4	0.77273	7173.57	28.0331	6.3422	0.22798	10.2943	0.05935	9.8313	0.06831
3.3	0.76744	4998.89	22.3502	6.3661	0.22664	10.1475	0.06158	9.8179	0.06819
3.2	0.76190	3598.36	17.3233	6.3923	0.22512	9.9961	0.06404	9.8047	0.06801
3.1	0.75610	2476.05	12.8706	6.4211	0.22338	9.8396	0.06674	9.7919	0.06777
3.0	0.75000	1446.86	9.21101	6.4531	0.22138	9.6774	0.06975	9.7796	0.06746
2.9	0.74359	692.632	6.71466	6.4890	0.21906	9.5088	0.07313	9.7680	0.06706
2.8	0.73684	325.643	5.27798	6.5297	0.21633	9.3327	0.07695	9.7574	0.06655
2.7	0.72973	173.764	4.45141	6.5766	0.21308	9.1475	0.08134	9.7481	0.06591
2.6	0.72222	106.141	3.92699	6.6317	0.20915	8.9513	0.08646	9.7406	0.06510
2.5	0.71429	71.9182	3.55954	6.6981	0.20429	8.7406	0.09257	9.7356	0.06410
2.4	0.70588	52.5214	3.28159	6.7817	0.19804	8.5094	0.10011	9.7338	0.06285
2.3	0.69697	40.5057	3.05917	6.8949	0.18950	8.2453	0.11002	9.7365	0.06128
2.2	0.68750	32.5327	2.87357	7.0776	0.17591	7.9080	0.12503	9.7454	0.05931

In order to search for trapping polytropes having physical relevance, we have to compare the characteristic radii of the trapping zone r_c and r_b to the r_{extr} radius, giving a limit on the physical relevance of the polytropic sphere. This can be done using the results presented in Table I for the central density $\rho_c = 5 \times 10^{15}$ g cm^{-3}. We can see that the gravitational mass and the surface radius of the relativistic polytropes significantly exceed the mass and radii related to the observed neutron stars; the discrepancy strongly increases with increasing polytropic index n. On the other hand, the limiting radius r_{extr} is for all considered values of n, quite comparable to the observed radii of neutron stars ($r_{extr} < R_{min}$). For all values of n, the central radius of the trapping zone $r_c < r_{extr}$, thus guaranteeing that the trapping is possible for all considered polytropes. However, $r_b < r_{extr}$ only for the polytropes with $n < 3.1$. The whole trapping zone will be contained in the allowed region only for these polytropic spheres.

We can also see that the energy density at the loci of the stable circular geodesic is on the level of $10^{-1}\rho_c$, but only on the level of $10^{-2}\rho_c$ at the unstable circular null geodesic, giving the outer edge of the trapping zone. Of course, the energy ratio depends significantly on the values of the spacetime parameters n, σ, ρ_c, as demonstrated in Table I. On the other hand, the ratio $\varrho(r_{extr})/\varrho_c \sim 0.07$ with only a slight dependence on n.

In order to illustrate the situation of physical relevance of the trapping zones, in Fig. 5 we give the functions $m(r_c; n, \sigma_{max})$ and $m(r_b; n, \sigma_{max})$, and in Fig. 6 we give the functions $r_c(n, \sigma_{max})$, $r_b(n, \sigma_{max})$ and $r_{extr}(n, \sigma_{max})$. In order to have good insight into the character of the trapping polytropes, we also give the functions $\rho(r_c)/\rho_c(n, \sigma_{max})$, $\rho(r_b)/\rho_c(n, \sigma_{max})$, and $\rho(r_{extr})/\rho_c(n, \sigma_{max})$ in Fig. 7. We give these functions for three characteristic selections of the central density: $\varrho_c = 10^{15}$, 5×10^{15}, 10^{16} g cm^{-3}. The numerical results show that all of the trapping zones are located under r_{extr} for all the polytropes with $n \leq 4$, if $\rho_c = 10^{16}$ g cm^{-3}. On the other hand, all of the trapping zones are located above r_{extr} for all the polytropes with $n \leq 4$, if $\rho_c = 10^{15}$ g cm^{-3}—in this case, the trapping effect should be physically implausible. In the intermediate case of $\varrho_c \sim 5 \times 10^{15}$ g cm^{-3}, the trapping zones can be fully contained in polytropes with $n \leq 3$. For $n > 3$, the trapping zones reach the polytrope surface at r_{extr}.

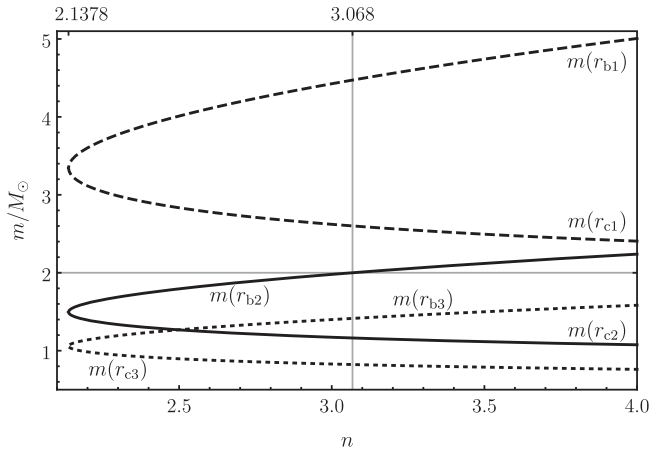

FIG. 5. The mass of the trapping polytropes with $\sigma = \sigma_{max}$, contained under the radius of photon circular orbits r_c and r_b, is given, depending on the polytropic index n, for three central densities ϱ_c: (1) 10^{15} g cm^{-3} (dashed lines), (2) 5×10^{15} g cm^{-3} (solid lines), and (3) 10^{16} g cm^{-3} (dotted lines).

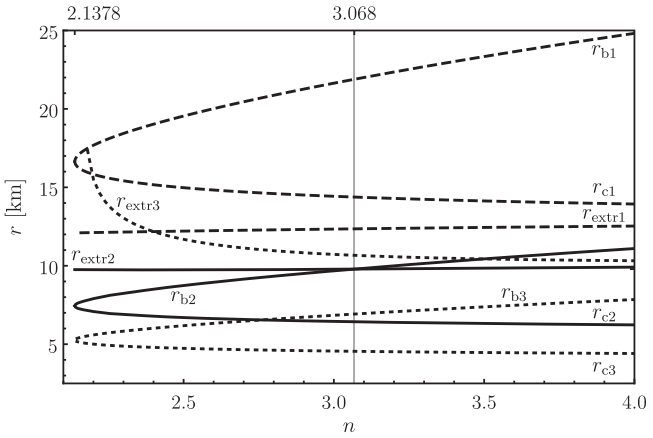

FIG. 6. Position of the null geodesics stable r_c and unstable r_b radii and the limit radius r_{extr}, depending on the polytropic index n, is given for the polytropes with three central densities ϱ_c: (1) 10^{15} g cm^{-3} (dashed lines), (2) 5×10^{15} g cm^{-3} (solid lines), and (3) 10^{16} g cm^{-3} (dotted lines). For the last case and $n < 2.17$, the polytropic balls have mass $M < 2M_\odot$; therefore, r_{extr3} does not exist for such values of n.

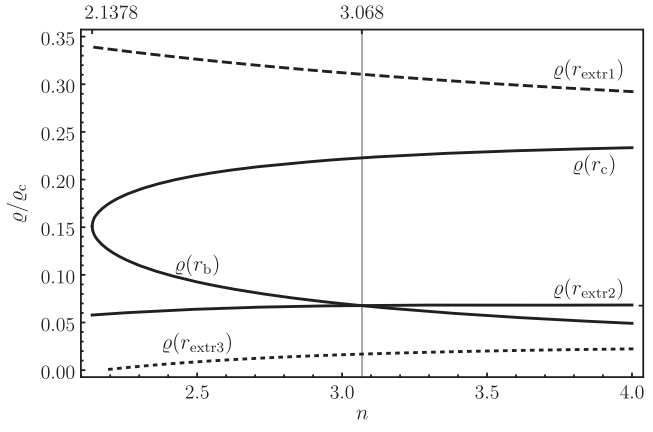

FIG. 7. Trapping polytropes with $\sigma = \sigma_{max}$. Energy density located at the null geodesics and loci of r_{extr}, depending on the polytropic index n, is given for three central densities ϱ_c: (1) 10^{15} g cm^{-3} (dashed lines), (2) 5×10^{15} g cm^{-3} (solid lines), and (3) 10^{16} g cm^{-3} (dotted lines). The functions $\varrho(r_c)/\varrho_c$ and $\varrho(r_c)/\varrho_c$ are the same for all three depicted cases. For the last case and $n < 2.17$, the polytropic balls have mass $M < 2M_\odot$.

C. Effective potential of null geodesics

We test the validity of our results, based on the study of the embedding diagrams of the optical geometry of the polytropic spheres, by using the direct study of the effective potential of the null geodesics that gives all of the information on the trapping zones [2].

The four-momentum p^μ of particles moving along null geodesics satisfies the geodesic equation (λ is an affine parameter)

$$\frac{\mathrm{D}p^\mu}{\mathrm{d}\lambda} = 0, \tag{52}$$

simultaneously with the normalization condition

$$p^\mu p_\mu = 0. \tag{53}$$

Because of the spherical symmetry of the internal metric studied, the motion plane is central, and for a single-particle motion, it is reasonable to choose the equatorial plane ($\theta = \pi/2$). Moreover, axial symmetry and time independence of the metric induce the existence of two Killing vector fields, resulting in conserved energy and axial angular momentum of the particle,

$$E = -p_t, \qquad L = p_\psi. \tag{54}$$

Then, the radial component of the geodesic motion, derived using (53), has to fulfill the relation

$$(p^r)^2 = e^{-2(\Phi+\Psi)}E^2\left(1 - e^{2\Phi}\frac{\ell^2}{r^2}\right), \tag{55}$$

where $\ell \equiv L/E$ is the impact parameter. For both the internal and external spacetime of the polytropic sphere, the turning points of the radial motion can thus be expressed by an effective potential V_{eff} with respect to the impact parameter. The motion is then allowed in regions where the impact dimensionless parameter $\tilde{\ell}$ satisfies the condition

$$\tilde{\ell}^2 \equiv \frac{\ell^2}{\mathcal{L}^2} \leq V_{\mathrm{eff}}^{\mathrm{int/ext}} \equiv \frac{\xi^2}{\exp(2\Phi_{\mathrm{int/ext}})}. \tag{56}$$

In the polytrope interior with parameters (n, σ), the effective potential $V_{\mathrm{eff}}^{\mathrm{int}}$ is determined by the metric coefficient $g_{\mathrm{tt}}(\xi; n, \sigma)$ with its radial profile fully governed by the function $\theta(\xi; n, \sigma)$.

The condition for the existence of the local maxima and minima of the internal spacetime effective potential, $\mathrm{d}V_{\mathrm{eff}}^{\mathrm{int}}/\mathrm{d}\xi = 0$, determines the loci of the null circular geodesics in terms of the equation

$$\theta(\xi) + (n+1)\xi\frac{\mathrm{d}\theta(\xi)}{\mathrm{d}\xi} = -\frac{1}{\sigma}. \tag{57}$$

For a given polytrope index n, the limiting case corresponding to coalescence of the radii of the circular null geodesics at an inflexion point of the effective potential, determined by the condition $\mathrm{d}^2V_{\mathrm{eff}}^{\mathrm{int}}/\mathrm{d}\xi^2 = 0$ implying the relation

$$1 + \sigma\left\{\sigma\theta(\xi)^2 + (n+1)\xi\left[\frac{\mathrm{d}\theta(\xi)}{\mathrm{d}\xi}\left(4 + (2n+1)\sigma\xi\frac{\mathrm{d}\theta(\xi)}{\mathrm{d}\xi}\right) + \xi\frac{\mathrm{d}^2\theta(\xi)}{\mathrm{d}\xi^2}\right] + \theta(\xi)\left[2 + (n+1)\sigma\xi\left(4\frac{\mathrm{d}\theta(\xi)}{\mathrm{d}\xi} + \xi\frac{\mathrm{d}^2\theta(\xi)}{\mathrm{d}\xi^2}\right)\right]\right\} = 0, \tag{58}$$

gives the minimal allowed value of the relativistic parameter $\sigma_{\mathrm{min}}(n)$. For a given $n > 2.138$, allowing the existence of the circular null geodesics, we can find the minimal value of the relativistic parameter $\sigma_{\mathrm{min}}(n)$ due to simultaneously solving the condition for an inflexion point of the effective potential; with the extrema relation given by Eq. (57), we obtain a simple relation governing $\sigma_{\mathrm{min}}(n)$ in the form

$$(n+2)\frac{\mathrm{d}\theta(\xi)}{\mathrm{d}\xi} + (n+1)\xi\frac{\mathrm{d}^2\theta(\xi)}{\mathrm{d}\xi^2} = 0. \tag{59}$$

The two solutions of Eq. (57) for given n and $\sigma \in (\sigma_{\mathrm{min}}, \sigma_{\mathrm{max}} \equiv n/(n+1))$ give the stable circular null geodesics located at r_{c}, where $\mathrm{d}^2V_{\mathrm{eff}}^{\mathrm{int}}/\mathrm{d}\xi^2 < 0$, and unstable circular null geodesics at r_{b}, where $\mathrm{d}^2V_{\mathrm{eff}}^{\mathrm{int}}/\mathrm{d}\xi^2 > 0$.

The effective potential $V_{\mathrm{eff}}^{\mathrm{int}}(\xi; n, \sigma)$ is constructed for the trapping polytropes with the index $n = 3$ for various values of relativistic parameters from the interval $\sigma_{\mathrm{min}}(n) < \sigma < \sigma_{\mathrm{max}}(n)$, illustrated in Fig. 8. The stable (unstable) null geodesics correspond to the local maxima (minima) of $V_{\mathrm{eff}}^{\mathrm{int}}$. Their positions are given by values of ξ close to 1 for the whole region of trapping. This means that for large configurations the trapping zones are located near the center, but for small configurations they are located near the surface. The exact ratio r_{c}/R is obtainable using Table I for selected values of n (for σ_{max}).

We demonstrate the dependence of the extension of the trapping zone on the parameter σ. The zone extension is given by the intersection of the line $V_{\mathrm{eff}}(r = r_{\mathrm{b}}(n, \sigma)) =$ const with the effective potential at $r < r_{\mathrm{c}}(n, \sigma)$, denoted as $r_{\mathrm{in}}(n, \sigma)$. The trapped null geodesics are restricted to the region $r_{\mathrm{in}}(n, \sigma) < r < r_{\mathrm{b}}(n, \sigma)$.

D. Local compactness radial profiles of the trapping polytropes

Finally, we consider the behavior of the compactness of the trapping polytropic spheres. We present the compactness of the total polytropic spheres and the compactness

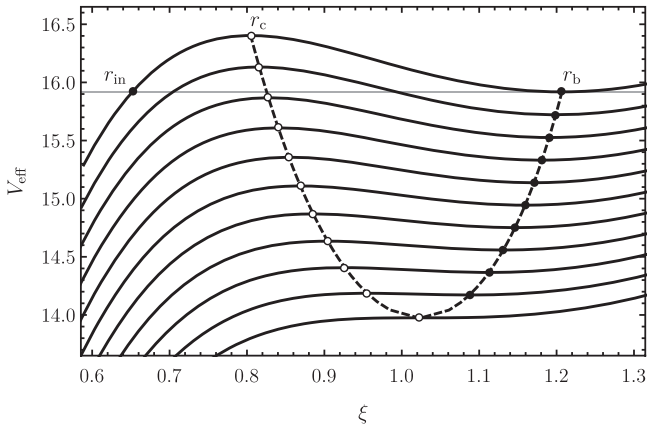

FIG. 8. The null geodesic effective potential $V_{\rm eff}^{\rm int}$ reflecting the trapping phenomenon for the polytrope spacetime having parameters from the trapping region in n–σ space. The effective potential is illustrated for the $n = 3$ polytropes. The parameter σ is evenly distributed between its maximum and minimum values. For each pair $\{n, \sigma\}$, loci of the stable and unstable circular null geodesics are marked. The $r_{\rm in}$ radius is constructed for the $\sigma = \sigma_{\rm max}$ effective potential.

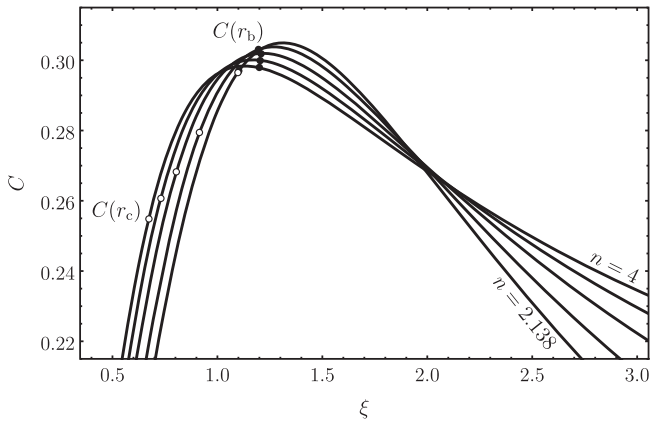

FIG. 9. The radial profiles of the local compactness in the region of trapping and in its vicinity. Profiles are plotted for $n \in \{2.138, 2.5, 3, 3.5, 4\}$ and the corresponding maximal value of σ. On each of the local compactness profiles, loci of the stable and unstable circular null geodesics are marked.

related to their interior at $r_{\rm c}$, $r_{\rm b}$, and $r_{\rm extr}$ for the polytropes with a maximal relativistic parameter and for the central density $\rho_{\rm c} = 5 \times 10^{15}$ g cm^{-3} in Table II. We can see that the compactness of the complete polytropes is very small, especially for n close to $n = 4$. However, surprisingly, even the compactness inside the polytrope at the center of the trapping zone ($r_{\rm c}$) and its outer boundary ($r_{\rm b}$) is not close to the critical value of $C = 1/3$. We always have $C(n, \sigma_{\rm max}) < C(r_{\rm c}(n, \sigma_{\rm max})) < C(r_{\rm b}(n, \sigma_{\rm max}))$.

TABLE II. List of compactness parameters describing a polytropic fluid sphere of a given n having $\sigma = \sigma_{\rm max}$. Compactness $C(R)$, $C(r_{\rm c})$ and $C(r_{\rm b})$ are independent on the central density $\varrho_{\rm c}$. Values of $C(r_{\rm extr})$ are calculated for central density $\varrho_{\rm c} = 5 \times 10^{15}$ g cm^{-3}.

n	$\sigma_{\rm max}$	$C(R)$	$C(r_{\rm c})$	$C(r_{\rm b})$	$C(r_{\rm extr})$
4.0	0.80000	9.88×10^{-6}	0.25492	0.29788	0.29794
3.9	0.79592	4.08×10^{-5}	0.25595	0.29829	0.29834
3.8	0.79167	2.55×10^{-5}	0.25703	0.29872	0.29874
3.7	0.78723	0.00124	0.25817	0.29914	0.29915
3.6	0.78261	0.00297	0.25937	0.29956	0.29956
3.5	0.77778	0.00454	0.26065	0.29998	0.29998
3.4	0.77273	0.00577	0.26199	0.30040	0.30039
3.3	0.76744	0.00660	0.26342	0.30081	0.30080
3.2	0.76190	0.00711	0.26493	0.30121	0.30120
3.1	0.75610	0.00768	0.26655	0.30160	0.30160
3.0	0.75000	0.00940	0.26828	0.30197	0.30198
2.9	0.74359	0.01432	0.27014	0.30230	0.30233
2.8	0.73684	0.02393	0.27215	0.30260	0.30266
2.7	0.72973	0.03783	0.27434	0.30283	0.30295
2.6	0.72222	0.05463	0.27673	0.30299	0.30318
2.5	0.71429	0.07308	0.27939	0.30301	0.30334
2.4	0.70588	0.09226	0.28241	0.30283	0.30340
2.3	0.69697	0.11152	0.28595	0.30228	0.30331
2.2	0.68750	0.13043	0.29057	0.30084	0.30304

One could intuitively expect that the compactness inside the region where the trapping effect occurs is high and maximal near the radius $r_{\rm c}$. However, this is not true, as seen in Fig. 9, which gives the dimensionless radial profiles of the compactness function $C(\xi)$ for selected values of n and a related maximal value of σ.

It is explicitly demonstrated that the maximal values of the compactness function $C(\xi)$ occur near (slightly above) the outer edge of the trapping zone and never cross the critical value of $C = 1/3$. The maximal value of the compactness function increases with a decreasing value of the polytropic index n. It seems that the trapping phenomenon is ruled by the strong gradient of the compactness function $C(r)$ rather than by the compactness itself.

VI. CONCLUSIONS

In our study we demonstrate the existence of standard general relativistic polytropes containing a zone of trapped null geodesics. The trapping polytropes can exist if the polytropic index $n \geq 2.1378$ and if the relativistic parameter σ is sufficiently high but lower than the maximal value given by the causality limit. The critical value of the relativistic parameter related to the $n = 2.1378$ polytrope reads $\sigma_{\rm max} = 0.681$. For the whole range of polytropic indices, the trapping zone cannot exist, if $\sigma < 0.677$.

Estimates on limits on the polytropic indices are presented for some equations of state in Ref. [25]. The possibility of applying different polytropic equations of state in different regions of the neutron star radial profile is mentioned in Ref. [25]. Moreover, our preliminary searches indicate the existence of the trapping zones in neutron star models related to sufficiently realistic equations of state.

The trapping polytropes do not fulfill the standard requirement on the existence of extremely compact objects, stating that the surface has to be located under the photon circular orbit of the external spacetime, and $C > 1/3$, established for the configurations with uniformly distributed energy density [2]. We have demonstrated the inverse—the compactness parameter can be much lower than the critical value of $C = 1/3$. Moreover, even the local compactness radial profile $C(\xi)$ does not reach this critical value, and its maximum lies outside the trapping zone. Seemingly, the gradient of the local compactness functions is decisive for the occurrence of the trapping effect.

We have considered if the existence of trapping polytropes could be physically relevant, namely, in the case of neutron stars. Thus, we assumed the applicability of the polytropic equation of state up to the region where the gravitational mass of the polytropic configuration reaches the value of $M = m(r_{\rm extr}) = 2M_\odot$, given by the recent observational restrictions on the neutron star mass. The trapping polytropes representing neutron stars can exist if the trapping zone is located under the radius of applicability, $r_{\rm extr}$. We have shown that the trapping $n = 3$ polytropes can exist if the central energy density reaches the value of $\rho_c = 5 \times 10^{15}$ g cm^{-3}.

The trapping zones of the polytropes with index $n = 3$ (or $n \sim 3$) could be expected to give an astrophysically relevant illustration of the effect of trapped null geodesics, as the $n = 3$ polytropes correspond to the ultrarelativistic degenerated Fermi gas, which could serve as an astrophysically relevant basic approximation of matter in the central parts of neutron stars [9]. Moreover, it is known that the realistic equations of state could be, at least partially, approximated by the polytropic equations of state [25–27].

We expect that the trapping zones of the general relativistic polytropes could be relevant in the trapping of neutrinos and related cooling of neutron stars, or in the case of trapping of gravitational waves.

Stability of the trapping polytropes will be studied in a forthcoming paper. Of course, it could also be interesting to study the possibility of the existence of trapping zones in polytropes governed by alternative gravitational theories and, especially, in neutron stars governed by the recently considered realistic equations of state.

ACKNOWLEDGMENTS

Z. S. and J. H. has been supported by the Albert Einstein Centre for Gravitation and Astrophysics financed by the Czech Science Agency Grant No. 14-37086G. J. N. and Z. S. were supported by the Silesian University in Opava, Internal Grant No. SGS/14/2016.

[1] M. A. Abramowicz, Phys. Rep. **311**, 325 (1999).
[2] Z. Stuchlík, J. Hladík, M. Urbanec, and G. Török, Gen. Relativ. Gravit. **44**, 1393 (2012).
[3] Z. Stuchlík, Acta Phys. Slovaca **50**, 219 (2000).
[4] Z. Stuchlík, S. Hledík, J. Šoltés, and E. Østgaard, Phys. Rev. D **64**, 044004 (2001).
[5] C. G. Böhmer, Gen. Relativ. Gravit. **36**, 1039 (2004).
[6] J. Hladík and Z. Stuchlík, J. Cosmol. Astropart. Phys. 7 (2011) 012.
[7] J. M. Lattimer and M. Prakash, Nucl. Phys. **A777**, 479 (2006).
[8] Z. Stuchlík, S. Hledík, and J. Novotný, Phys. Rev. D **94**, 103513 (2016).
[9] S. L. Shapiro and S. A. Teukolsky, *Black Holes, White Dwarfs and Neutron Stars: The Physics of Compact Objects* (John Wiley & Sons, New York, 1983), p. 672.
[10] Z. Stuchlík, Bull. Astron. Inst. Czech. **34**, 129 (1983).
[11] Z. Stuchlík and S. Hledík, Phys. Rev. D **60**, 044006 (1999).
[12] Z. Stuchlík, Mod. Phys. Lett. A **20**, 561 (2005).
[13] Z. Stuchlík, S. Hledík, and J. Juráň, Classical Quantum Gravity **17**, 2691 (2000).
[14] R. F. Tooper, Astrophys. J. **140**, 434 (1964).
[15] C. W. Misner, K. S. Thorne, and J. A. Wheeler, *Gravitation* (W.H. Freeman and Co., San Francisco, 1973).
[16] M. A. Abramowicz, B. Carter, and J. P. Lasota, Gen. Relativ. Gravit. **20**, 1173 (1988).
[17] M. A. Abramowicz, Mon. Not. R. Astron. Soc. **245**, 733 (1990).
[18] M. A. Abramowicz, J. C. Miller, and Z. Stuchlík, Phys. Rev. D **47**, 1440 (1993).
[19] J. Kovář and Z. Stuchlík, Classical Quantum Gravity **24**, 565 (2007).
[20] O. Semerák, Nuovo Cimento B **110**, 973 (1995).
[21] Z. Stuchlík, G. Török, S. Hledík, and M. Urbanec, Classical Quantum Gravity **26**, 035003 (2009).
[22] J. M. Lattimer, Gen. Relativ. Gravit. **46**, 1713 (2014).
[23] N. Chamel, P. Haensel, J. L. Zdunik, and A. F. Fantina, Int. J. Mod. Phys. E **22**, 1330018 (2013).
[24] J. M. Lattimer and M. Prakash, Phys. Rep. **621**, 127 (2016).
[25] J. S. Read, B. D. Lackey, B. J. Owen, and J. L. Friedman, Phys. Rev. D **79**, 124032 (2009).
[26] F. Özel and D. Psaltis, Phys. Rev. D **80**, 103003 (2009).
[27] A. W. Steiner, J. M. Lattimer, and E. F. Brown, Astrophys. J. **722**, 33 (2010).